# Axisymmetric shapes and forces resulting from the interaction of a particle with a solidifying interface

L. Hadji
*Mathematics Department, The University of Alabama, Tuscaloosa, Alabama 35487-0350*
(Received 6 May 2002; published 21 October 2002)

A steady state model of the interaction of a foreign particle with a solidifying interface in a microgravity environment is presented in order to examine the phenomenon of particle engulfment. The model considers the interception of a spherical impurity particle by a deformable solid-liquid interface. Three forces are present whenever the particle is in near contact with the solid front, namely, the disjoining pressure force, the thermal force, and the hydrodynamic pressure force. These forces arise due to (i) the disjoining pressure gradients resulting from the deformation of the interface behind the particle, (ii) the interface distortion caused by the difference between the coefficients of thermal conductance of the particle and melt, and (iii) the hydrodynamic pressure resulting from the melt flow driven by the pressure gradients in the gap between the particle and the interface. The model accounts for the modification of the melt's freezing point by these pressure terms. The dependence of the interface morphology on the various physical and processing parameters is revealed. These include the rate of solidification, the thermal gradient, the gap width, and the coefficients of thermal conductivity of the particle and the melt. The gap profile is calculated and used in the evaluation of the three forces that characterize the interaction. The analysis shows that the outcome of the interaction, i.e., particle engulfment or rejection, depends primarily on the competition between the hydrodynamic and thermal forces.

DOI: 10.1103/PhysRevE.66.041404 PACS number(s): 82.70.−y, 64.70.Dv, 81.30.Fb, 81.05.Ni

## I. INTRODUCTION

The understanding of the interaction between particles suspended in the melt and a crystallization front is important to the fabrication of particulate metal matrix composites [1] and to other natural and man-made processes [2–5]. This interaction has proven to be very difficult to quantify. A lot of progress has been made towards its understanding through experiments, computer simulations, and theoretical analyses. However, many relevant questions remain unanswered. The reader is referred to the papers by Chernov and Temkin [6] and Li and Neumann [7] for reviews of the problem.

The presence of a foreign particle near a solidifying interface induces locally a slight change in the melting point of the substance, and in turn the modification of the melting point induces a change in the shape of the solid-liquid interface. Three factors are responsible for this change: (i) the difference in the thermal conductivities of the melt and particle, (ii) the disjoining pressure, and (iii) the hydrodynamic pressure. The latter two take place in the melt film separating the particle from the front. The understanding of the dependence of the front's deformation on the material and processing properties is essential to the understanding of the interaction of the particles with the advancing solid-liquid interface. The quantification of the influence of the particle's presence on the shape of the interface in terms of the physical and processing parameters has not been fully resolved and its determination remains an intensive area of research. The interaction of a foreign particle with a growing crystallization front and the resulting interfacial morphologies are influenced by the following three factors.

### A. Thermal effects

The influence of the thermal factors on the particle-interface interaction has been investigated by numerous scientists. The first experimental inquiry into the role of the thermal effects on the capture of particles by growing crystals was conducted by Zubko *et al.* [8]. They examined the solidification, by the Bridgman method, of three materials (bismuth, tin and zinc) that have been mixed with particles of different material (tungsten, iron, molybdenum, nickel, chromium, and tantalum). The experiments demonstrated that the nature of the interaction depended primarily on the relative magnitudes of the coefficients of thermal conductivity of the particle ($k_p$) and the melt ($k_l$). They found that the particle is captured if $k_p > k_l$ and rejected by the solid front if $k_p < k_l$, regardless of the wetting properties of the particles. These authors accounted for the strong dependence of the coefficients of thermal conductivity on temperature, but did not offer a physical explanation for the behavior of the particles at the interface. Later theoretical and experimental studies found that the crystal behind the particle bulges into the melt if $k_p < k_l$ and forms a trough otherwise [9]; and then tried to explain the rejection and the engulfment of the particle in terms of the interface profile, i.e., the formation of a depression is conducive to engulfment while the formation of a bump is conducive to pushing. Hadji [10] has shown that the presence of a foreign spherical particle near a solid-liquid interface gives rise to a thermal force that acts on the particle. This force is given by

$$F_{TH} = \frac{2\pi L G a^3 (1-\alpha)}{(2+\alpha) T_m}, \tag{1}$$

where $L$ is the latent heat of fusion per unit volume, $G$ is the imposed thermal gradient in the melt, $a$ is the particle's radius, $T_m$ is the melting point of the fluid, and $\alpha = k_p / k_l$. The derivation of the thermal force is discussed in Sec. IV. The experimental findings [8] can easily be interpreted in terms of the thermal force; the influence of the thermal conductiv-

 

ity contrast, represented by the parameter $\alpha$, is such that the thermal force pushes the particle against the front if $\alpha>1$ and rejects the particle away from the front if $\alpha<1$. Furthermore, the analysis [10] shows that the thermal force is of the same order of magnitude as the other forces that are usually accounted for in the studies involving the interaction of particles with an advancing solid-liquid interface.

### B. Disjoining pressure effects

Chernov *et al.* [6,11] have used the concept of disjoining pressure to describe how a particle can be rejected by a moving interface. If the disjoining pressure is from van der Waals interactions, then it is expressed as $-\mathcal{A}/6\pi g^3$ and the induced force is given by

$$F_{DP}=\frac{\mathcal{A}}{3}\int_0^\infty \frac{r dr}{g^3(r)}, \tag{2}$$

where $\mathcal{A}$ is the Hamaker constant and $g(r)$ denotes the profile of the gap separating the particle from the deformed solid-liquid interface.

### C. Hydrodynamic pressue effects

The pressure gradients that develop in the gap as a result of the particle's presence near the interface and the subsequent deformation of the solid front due to the thermal effects drive the melt to flow. If the melt is treated as a Newtonian fluid then the melt flow is described by the lubrication equation [12]

$$\frac{\partial^2 u}{\partial z^2}=\frac{1}{\mu}\frac{\partial P}{\partial r},$$

where $u(z)$ is the radial component of the melt's velocity, $\mu$ is the dynamic viscosity of the fluid, and $P(r)$ is the pressure. Applying the no-slip boundary conditions at the interface, $h(r)$, and at the particle-melt boundary, $S(r)=h_\infty+a-\sqrt{a^2-r^2}$ $(r\leqslant a)$, leads to

$$u(z)=\frac{1}{2\mu}\frac{\partial P}{\partial r}[z^2-(S+h)z+Sh].$$

On neglecting any changes in the melt's density upon solidification, the conservation of mass equation

$$2\pi r\int_h^S u(z)dz=-\pi r^2 V,$$

then implies

$$P(r)=-6\mu V\int_0^r \frac{\zeta d\zeta}{g^3(\zeta)},$$

where, for convenience in the numerical simulations, the limits of integration are chosen so that $P(0)=0$. The drag force is then given by [6,7,13,14],

$$F_{drag}=\int_0^\infty 2\pi r P(r)dr=-12\mu V\int_0^\infty \pi r\int_0^r \frac{x dx}{g^3(x)}dr. \tag{3}$$

The inclusion of the shrinkage flow will modify Eq. (3) by a small factor whose magnitude is $O(\rho_s/\rho_l)$, where $\rho_s$ and $\rho_l$ are the densities of the solid and liquid phase, respectively.

In this paper the estimation of the forces [10], which considers a planar solid-liquid interface, is revisited to include the effects of the disjoining pressure and the hydrodynamic pressure on the shape of the solid-liquid interface. Only then can a reasonable assessment of the forces be made. An attempt at this problem has been made by Sasikumar *et al.* [15] and Casses and Azouni [16]. However, these authors use an expression for the temperature which does not satisfy the heat conduction equation in the cylindrical geometry and does not even have the proper power of the coordinates $z$ and $r$ as either $z$ or $r\rightarrow\infty$. Sasikumar and Ramamohan [17] correct their results [15] but present an incomplete analysis of the front shape and forces on the particle. Recently, there have been several investigations of the interface profile near a particle; the experiments of Sen *et al.* [18] depict *in situ* and real-time evolution of the solid-liquid interface morphology in the vicinity of a particle or void. In particular, the dependence of the shape of the interface shape on $\alpha$ is thoroughly analyzed. Hadji [19] carried out an asymptotic analysis of the interface profile which results from the the dual effects of the disjoining pressure and interface curvature. The resulting interface profile is analyzed in Ref. [20] and found to exhibit a cusp at the origin when the particle is in the near-contact region. This finding is in agreement with the theory that predicted that the curvature of the profile has a logarithmic singularity. In the near-contact region, the interface behaves like $\text{const}+r^2\ln r$ as $r\rightarrow 0$. In the following analysis, we also include the hydrodynamic pressure and show that it has a strong influence on the shape of the interface. This prediction is in agreement with numerous experiments that show significant interfacial deformations caused by variations in the growth rate. Furthermore, the gap separation profile is calculated and used to evaluate the forces acting on the particle. However, neither the stability of the melt film nor the question of minimum film thickness at which the disjoining pressure becomes effective are addressed in this paper. The minimum gap width is considered an external parameter.

The plan for the remainder of this paper is stated as follows. The mathematical model as well as the major assumptions are presented in Sec. II. In Sec. III we solve the model and analyze the interface profile. The analysis is divided in two parts. The first part deals with a detailed analysis of the disjoining pressure effect and the second part includes the effects due to the solidification rate. An assessement of the forces is carried out in Sec. IV. The discussion of the results and conclusions are presented in Sec. V.

## II. MATHEMATICAL MODEL

Consider the situation illustrated in Fig. 1 which depicts an inert and spherical particle of radius $a$ placed in the pure

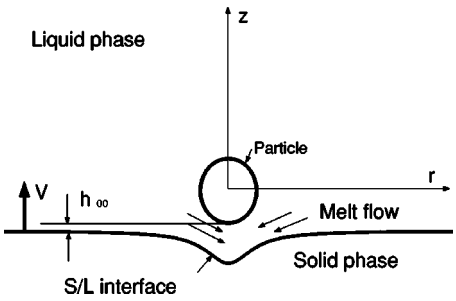


FIG. 1. Sketch of a deformed solid-liquid interface near a particle of radius $a$. The interface is moving with velocity $V$ in the positive $z$ direction; $h_\infty$ is the distance between the lowest point on the particle's surface and the planar interface (far away from the particle).

melt at a distance $h_\infty$ from the planar solid front. We consider an axisymmetric geometry with the radial coordinate axis, r, taken along the planar solid-liquid interface and the $z$ axis pointing vertically upward. If we write the heat conduction equation in a frame that is moving with velocity $V$ in the $z$ direction, and scale lengths by the particle's radius $a$, then the resulting equation consists of the Laplace's equation plus a convection term that is multiplied by the factor $aV/\kappa$, where $\kappa$ is the heat diffusion coefficient. Typically, $a$ varies between 1 and 100 $\mu$m, $V$ varies between 0.01 and 100 $\mu$m s$^{-1}$ and $\kappa \approx 10^{-5}$ m$^2$ s$^{-1}$. Thus the factor $aV/\kappa$ varies between $10^{-9}$ and $10^{-3}$ and so the convection term is negligible. Furhermore, we assume that (i) there is no change in heat conductivities upon solidification and (ii) the interface equilibrium temperature accounts for the change in the melt's melting point due to the undercooling effects of the disjoining pressure, the Gibbs-Thomson effect and the hydrodynamic pressure in the liquid film sandwiched between the particle's lower surface and the interface. Under these assumptions, the thermal field is described by the steady state form of the heat conduction equations in the melt and in the particle,

$$\frac{1}{r}\frac{\partial}{\partial r}\left(r\frac{\partial T}{\partial r}\right)+\frac{\partial^2 T}{\partial z^2}=0, \tag{4}$$

$$\frac{1}{r}\frac{\partial}{\partial r}\left(r\frac{\partial T_p}{\partial r}\right)+\frac{\partial^2 T_p}{\partial z^2}=0, \tag{5}$$

where $T$ and $T_p$ are the temperature in the liquid phase and in the particle, respectively. At the particle-melt boundary, $[z-(a+h_\infty)]^2+r^2=a^2$, the continuity of the temperature and of the heat flux implies

$$T=T_p, \quad \nabla(k_l T-k_p T_p)\cdot\mathbf{n}=0, \tag{6}$$

where $\mathbf{n}$ denotes the normal vector to the particle-melt boundary that is pointing into the liquid and $\nabla$ is the gradient vector. The interface equilibrium temperature is described by

$$T_I=T_m+\Delta T_{curv}+\Delta T_{DP}+\Delta T_{HP}, \tag{7}$$

where $\Delta T_{curv}$ is the curvature undercooling given by the Gibbs-Thomson formula [21,22]

$$\Delta T_{curv}=-\frac{\sigma_{sl}T_m}{L}\mathcal{K}. \tag{8}$$

In the near-contact region, the molecular interactions in the melt film contribute an amount $\Phi(g)$ to the free energy [12,23]. Following Chernov [6], we assume that $\Phi(g)$ arises from the nonretarded London–van der Waals interactions and has the form $\Phi(g)=\mathcal{A}/12\pi g^2$. The Hamaker constant $\mathcal{A}$ depends on the properties of the phases involved in the interaction but is assumed not to depend on the film thickness. The disjoining pressure in the film is $\mathcal{P}_{DP}=d\Phi/dg=-\mathcal{A}/6\pi g^3$, which gives rise to the undercooling term

$$\Delta T_{DP}=\frac{\mathcal{A}T_m}{6\pi L g^3(r)}. \tag{9}$$

The undercooling term due to the hydrodynamic pressure is given by

$$\Delta T_{HP}=-\frac{6\mu V T_m}{L}\int_0^r \frac{x}{g^3(x)}dx. \tag{10}$$

The symbols that appear in Eqs. (8)–(10) are defined as follows: $\sigma_{sl}$ is the surface excess free energy and $\mathcal{K}$ is the front's curvature (positive when the center of curvature lies on the solid side of the interface). The far-field condition is described by

$$\frac{\partial T}{\partial z}=G \quad \text{as} \quad z\to\infty. \tag{11}$$

On assuming that (i) the particle's diameter is small compared to the horizontal extent of the interface, (ii) the particle is in the near proximity of the solid-liquid interface, and (iii) the solid-liquid interface is deformable, we have from Eqs. (4)–(6) and (11),

$$T(r,z)=T_m+Gz-Ga^3\left(\frac{\alpha-1}{\alpha+2}\right)\frac{z-(h_\infty+a)}{\{[z-(h_\infty+a)]^2+r^2\}^{3/2}}. \tag{12}$$

Equation (12) applies only in the case considered here, i.e., the melt is a pure substance whose $T_m$ isotherm is deformed by the thermal conductance contrast. Note that if the interface is nondeformable, then the method of images must be used to solve for the temperature distribution whose value is $T_m$ at $z=0$. On evaluating Eq. (12) at $z=0$ and on using Eqs. (7)–(10), we obtain the differential equation

$$-\mathcal{K}=\frac{LGa^3}{T_m\sigma_{sl}}\left(\frac{\alpha-1}{\alpha+2}\right)H(r)-\left(\frac{\mathcal{A}}{6\pi g^3(r)\sigma_{sl}}-\frac{6\mu V}{\sigma_{sl}}\int_0^r\frac{x}{g^3(x)}dx\right)u(a-r), \tag{13}$$

where $g(r)=[h_\infty+a-\sqrt{|a^2-r^2|}-h(r)]$ is the gap separation, $h(r)$ is the interface profile, and $u(a-r)$ is the unit step function given by

$$u(a-r)=\begin{cases}1 & \text{if } r<a,\\ 0 & \text{if } r>a,\end{cases} \tag{14}$$

and

$$H(r)=\frac{h_\infty+a}{[(h_\infty+a)^2+r^2]^{3/2}}. \tag{15}$$

The unit step function is utilized to model the fact that both the disjoining pressure and the hydrodynamic pressure act only in the melt film between the particle and the interface. The dependence of the front's curvature on the interface profile is given by

$$\mathcal{K}=-\frac{h''(r)}{[1+(h')^2]^{3/2}}-\frac{h'(r)}{r[1+(h')^2]^{1/2}}, \tag{16}$$

where the prime notation pertains to derivative with respect to the variable $r$. On substituting Eq. (16) into Eq. (13), we obtain the following coupled system of nonlinear differential equations for the interface profile:

$$\frac{dh}{dr}=v(r),$$

$$\frac{dw}{dr}=u(a-r)\frac{r}{g^3(r)},$$

$$\frac{dv}{dr}=(1+v^2)^{3/2}\left[-\frac{v}{r}(1+v^2)^{-1/2}+\frac{a^3GL}{\sigma_{sl}T_m}\left(\frac{\alpha-1}{\alpha+2}\right)H(r)\right.$$
$$\left.-\left(\frac{\mathcal{A}}{6\pi\sigma_{sl}g^3(r)}-\frac{6\mu V}{\sigma_{sl}}w\right)u(a-r)\right], \tag{17}$$

where the intermediate variable $w$ is given by

$$w(r)=\int_0^r\frac{x\,dx}{g^3(x)}. \tag{18}$$

The system of equations (17) and Eq. (18) are complemented by the following conditions: the symmetry condition $v(0)=0$, $w(0)=0$, and the far-field condition $h(r)\to 0$ as $r\to\infty$. The later condition is due to the fact that far away from the particle, the solid-liquid interface is assumed to remain planar at the location $z=0$. We are, thus, assuming that the growth rates considered in this study are low enough that the possibility of the onset of morphological instabilities is remote. The system of equations (17) and corresponding initial and boundedness conditions are viewed as an initial value problem: the system is solved subject to an assumed value of $h(r)$ at $r=0$, $w(0)=0$, and the symmetry condition $h'(0)=0$. The correct value of $h(0)$ is that value which satisfies, theoretically, the condition at infinity, i.e., $h(r)\to 0$ as $r\to\infty$. In a numerical experiment, this condition must be applied at an $r$ location that is far enough from the origin to describe the far field behavior of the interface. At the same time, because the system is solved as an initial value problem, the range of the interval of integration must not be allowed to be very large. The numerical experiments carried out with several values of $h(0)$ and $h_\infty$ show that the shape of the interface depends solely on the value of the gap thickness at the origin, $g_0=h_\infty-h(0)$, and not on the specific values of $h_\infty$ and $h(0)$. Figure 2 depicts some typical patterns that are observed in the simulations. Note that there is a significant amount of deformation in the neighborhood of the particle with the interface becoming planar as we move away from the particle. The height reached by the planar portion of the interface depends on $g_0$ and on the numerical values of the physical parameters. The boundedeness condition, $h(r)\to 0$ as $r\to 0$, seems to be always satisfied. This is consistent with the mathematical model. However, from a numerical standpoint, the integration range must be taken very large to actually have, within discretization errors, $h(r)=0$. In our numerical experiments, we have arbitrarily used an integration range of about ten particle diameters. Furthermore, we circumvent the evaluation of the system (17) at the origin by the following procedure. Owing to the fact that $v(0)=0$ and $w(0)=0$, we have

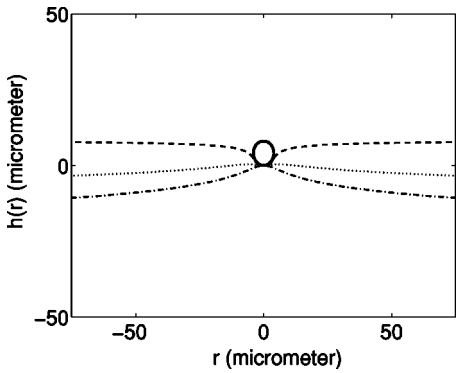


FIG. 2. Plot of a gas bubble of radius $a=4$ $\mu$m immersed in succinonitrile (SCN) and the interface profiles for three values of the growth rate, $V=0.0$ $\mu\text{ms}^{-1}$ (dash-dotted line), $V=15$ $\mu\text{ms}^{-1}$ (dotted line), and $V=30$ $\mu\text{ms}^{-1}$ (dashed line) over a horizontal extent of about 20 particle diameters.

$$\frac{dv}{dr}(0)=\frac{a^3GL}{\sigma_{sl}T_m}\left(\frac{\alpha-1}{\alpha+2}\right)H(0)-\frac{\mathcal{A}}{6\pi\sigma_{sl}[h_\infty-h(0)]^3}. \tag{19}$$

A forward difference formula for $dv/dr$ allows the evaluation of $v$ at a location $r=\delta>0$ very close to the origin. We have

$$v(\delta)=\delta\frac{a^3GL}{\sigma_{sl}T_m}\left(\frac{\alpha-1}{\alpha+2}\right)H(0)-\frac{\mathcal{A}}{6\pi\sigma_{sl}[h_\infty-h(0)]^3}. \tag{20}$$

We have set $\delta=10^{-20}$ and used the Matlab numerical ODE45 to solve Eq. (17) for $r>\delta$.

## III. INTERFACE PROFILE

In this section, we present an analysis of the influence of the particle's presence on the morphology of the interface. We consider two experimental setups. Experimental results are available for these systems under normal gravity conditions. The first one considers the solidification of succinonitrile (SCN) containing SiC particles and is characterized by a high value of the thermal conductivity ratio, $\alpha \approx 381$. The second one consists of gas bubbles in SCN and is characterized by $\alpha = 0$. From an experimental point of view, the bubbles contain air that was dissolved in the melt during the preparation of the sample. The numerical values for the physical constants are [24] $\mu = 2.6 \times 10^{-3}$ kg m s$^{-1}$, $G = 10\,800 - 30\,800$ K m$^{-1}$, $L = 4.6 \times 10^{7}$ J m$^{-3}$, $T_m = 328$ K, and $\sigma_{sl} = 0.03$ J m$^{-2}$. We consider a Hamaker constant $\mathcal{A} = 10^{-19}$ J. This numerical value of $\mathcal{A}$ is typical for liquid films for which the disjoining pressure results from the nonretarded van der Waals interactions. Furthermore, we assume that $\mathcal{A} > 0$ so that the force resulting from the disjoining pressure is repulsive, i.e., acts opposite to the drag force. The case $\mathcal{A} < 0$ is found to yield qualitatively similar results.

### A. Disjoining pressure effects

We begin our analysis of the possible shapes resulting from the interaction between the particle and the solid-liquid interface by focusing on the influence of the disjoining pressure. This is accomplished by turning off the effects of the hydrodynamic pressure ($V = 0$). The resulting system of equations (17) is solved over a horizontal extent of ten particle diameters. An initial value for the interface profile, $h(0)$, as well as a value for the gap thickness at the origin, $g_0$, are prescribed. This is accomplished by prescribing a value for $h_\infty$, the gap thickness is then $g_0 = h_\infty - h(0)$. In Figs. 3 and 4, where the interface-particle system is plotted for an SCN-SiC experimental setup, we note that for a relatively large gap width, $g_0 > 10$ Å, the interface profile is determined by the thermal factors, i.e., because $\alpha > 1$, the interface exhibits a concave shape and it almost conforms to the shape of the particle [10,19]. For $g_0 = 10$ Å, the disjoining pressure enters into play and induces interesting morphological changes. These are shown in Fig. 4. The peak shape that appears at the origin has been quantified by Hadji [20] in his analysis of the interface profile near a foreign spherical particle under the dual action of the undercoolings due to the disjoining pressure and curvature. It is found that $h(r) \sim \text{const} + r^2 \ln r$ as $r \to 0$ in the limit of a vanishingly small gap thickness. This implies a logarithmic singularity in the curvature. The peak in the interface profile resembles the dimple effect that is observed when two viscous drops come into close contact [25,26]. Away from the origin, the interface shape is determined by the thermal conductivity ratio $\alpha$. A different scenario holds for the case of SCN immersed with air bubbles shown in Figs. 5 and 6. For a large gap thickness, the interface is convex since $\alpha = 0$. Also in this case, the decrease in the gap width is associated with the appearance of a peak at the origin in the solid front's profile.

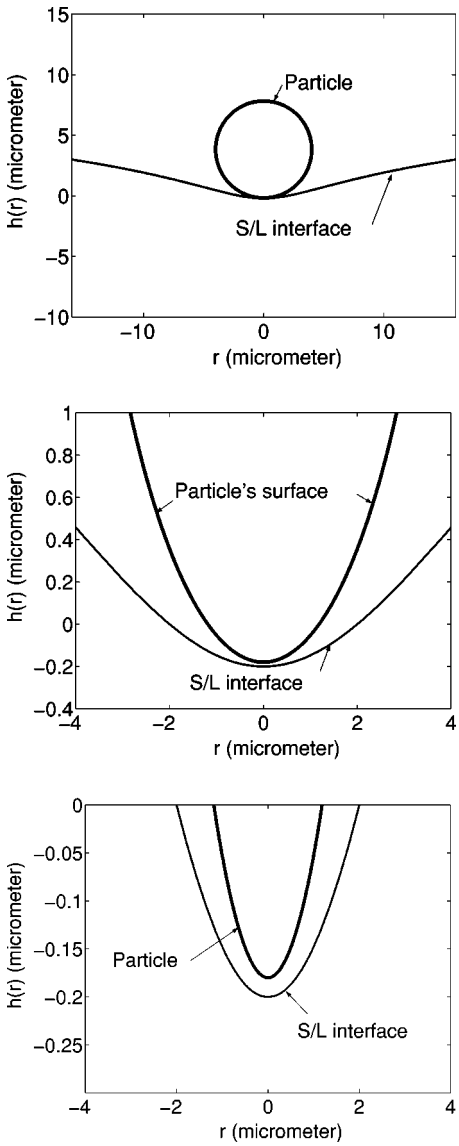


FIG. 3. Plot of $h(r)$ for the SCN-SiC system with $a = 4$ $\mu$m and for a gap thickness $g_0 = 100$ Å. The top figure depicts the particle's position over a horizontal extent of two particle diameters, while the corresponding middle and bottom figures are magnifications of the near-contact region.

### B. Growth rate effects

Consider now the effect of the growth rate on the front's morphology. The inclusion of the front's velocity in the analysis brings the effect of the hydrodynamic pressure into action. We are considering a steady situation wherein the gap separation at the origin, $g_0$, is kept fixed and the growth rate varied. For a given growth rate $V$, the interface profile that results from the solution of the system (17) corresponds to the profile that is observed experimentally when the solid front that is approaching the particle at a velocity $V$ is a distance $g_0$ from the particle. Figure 7 depicts the dependence of the interface morphology near the particle on the growth velocity for an SCN-SiC system. For a low growth rate, $V = 1$ $\mu$m s$^{-1}$, the front's profile still resembles that for $V = 0$ shown in Fig. 3. On a length scale comparable to the

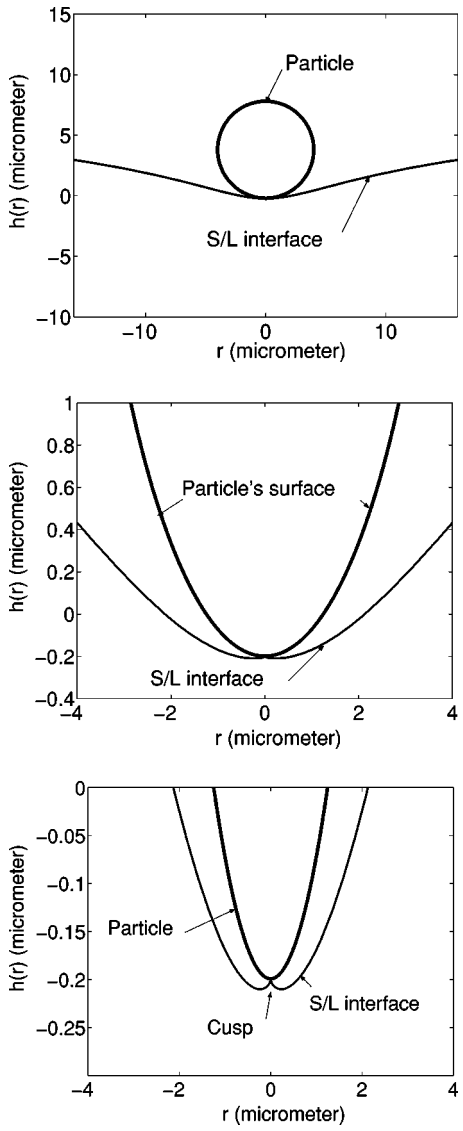


FIG. 4. Plot of $h(r)$ for the SCN-SiC system with $a=4$ $\mu$m and for a gap thickness $g_0=10$ Å. The top figure depicts the particle's position over a horizontal extent of two particle diameters, while the corresponding middle and bottom figures are magnifications of the near-contact region. Note the peak formation at the origin.

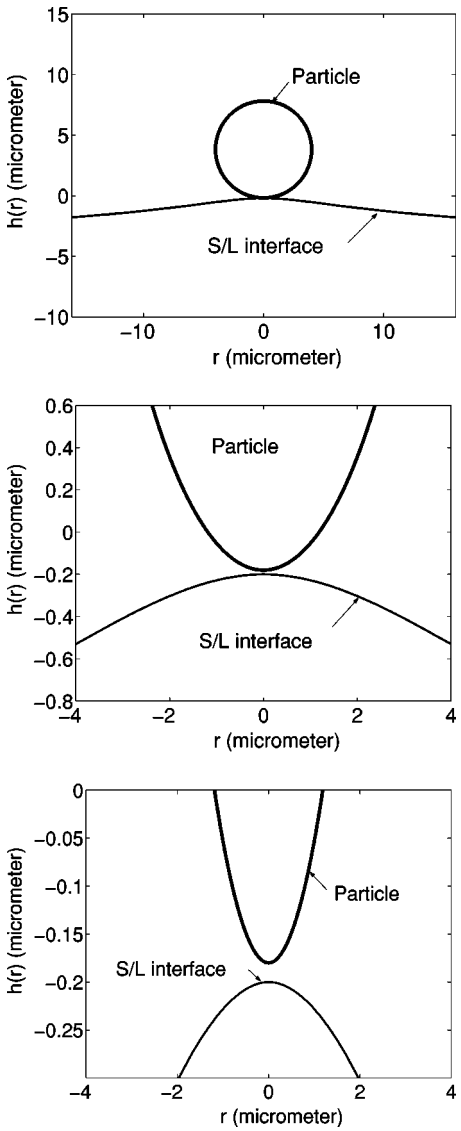


FIG. 5. Plot of $h(r)$ for a gas bubble of radius 4 $\mu$m immersed in SCN for a gap separation $g_0=100$ Å. The middle and bottom plots are magnifications of the top figure.

particle's radius, the profile is determined by the thermal factors, i.e. the thermal conductivity ratio $\alpha$, while on a length scale comparable to the gap thickness, the disjoining pressure is the determining factor of the profile at the origin. However, the magnification of the near-contact region does not reveal any dimple formation. As $V$ is increased to 18 $\mu$m s$^{-1}$, the depression in the front has deepened slightly with more solid surrounding the particle. This trend continues with increasing $V$ until the solid-liquid interface has surrounded the whole lower part of the particle, $z=h_\infty+a-\sqrt{a^2-r^2}$. Beyond this value for $V$, the mathematical model ceases to be valid since it accounts only for the physics that takes place in the melt sandwiched between the lower half of the particle and the interface. Figure 8 is a sequence showing the effect of increased growth rate for the case of an air bubble immersed in SCN. For very low velocity, the profile is defined by $\alpha$. As $V$ is increased further, a trough forms under the particle and the process of engulfment begins and continues until the lower portion of the particle is completely surrounded by the solid. This engulfment process is accompanied by changes in the gap thickness $g(r)$, which are plotted in Fig. 9. Note that the gap thickness away from the origin decreases with increasing growth rates and does not conform to the shape of the particle. Thus, the assumption of a parabolic profile for the gap width or the interface, which is often used, is incorrect. Furthermore, we observe that the gap separation changes with $V$ even in the neighborhood of the origin. Hence the often used assumption that the interface shape is primarily determined by the disjoining pressure near the origin is also incorrect. Due to a lack of pertinent microgravity results, we validate the present model against the ground experiments carried out by Stefanescu *et al.* [24]. Indeed, these authors have conducted several experiments using several types of particles mixed with the transparent or-

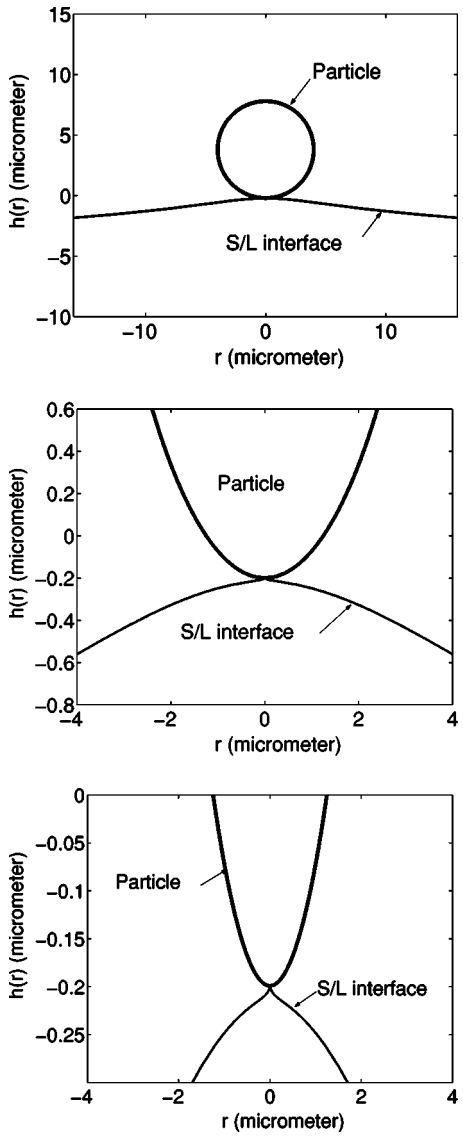


FIG. 6. Plot of $h(r)$ for a gas bubble of radius 4 $\mu$m immersed in SCN for a gap separation $g_0=10$ Å. The middle and bottom plots are magnifications of the top figure. Note the peak formation at the origin.

ganic material SCN. In those experiments involving SiC particles dispersed in SCN, they have observed that a particle of radius 4 $\mu$m was pushed at a solidification rate of 9.2 $\mu$m s$^{-1}$. They recorded the following sequence of events (Fig. 5 in Ref. [24]): as the interface intercepts the particle, a very shallow trough forms on the part of the solid front underlying the particle. As the solidification rate is increased, the trough got deeper and more solid surrounds the particle as if whenever any part of the interface touches the particle it ceases to move. This sequence of events resembles the patterns shown in Fig. 7.

Their experiments involving the solidification of succinonitrile in the presence of air bubbles (see Fig. 11 of Ref. [24]) yielded the following sequence of events. At low growth rates, a bump formed on the interface as the air bubble is approached, then a depression formed on the elevated part of the interface as $V$ is increased. As the interface is driven at a

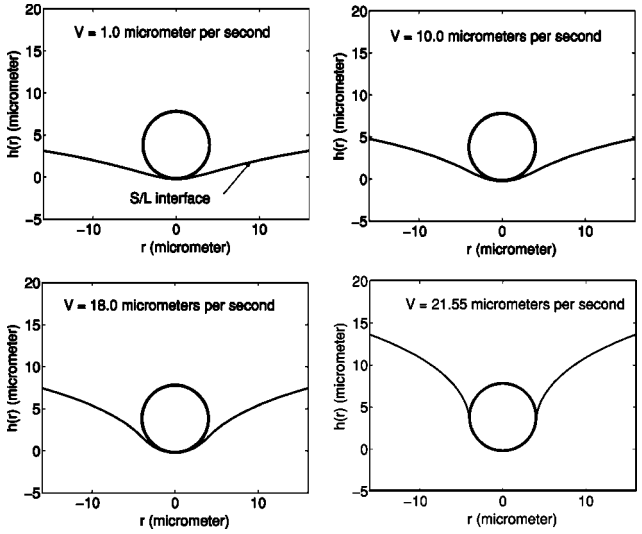


FIG. 7. Changes in the interface profile near the particle as function of the growth velocity $V$ for an SCN-SiC system ($\alpha=381$); $a=4.0$ $\mu$m and $g_0=20$ Å.

higher growth rate, the trough widened and engulfed more of the particle, in agreement with the predictions of the present model shown in Fig. 8.

## IV. FORCES

The preceding section dealt with the analysis of the steady axisymmetric interface shapes near a foreign particle. It showed that the presence of a particle near a solidifying front is associated with several different interface profiles, depending on the values of the growth rate, the disjoining pressure, the thermal conductivity ratio, and the gap thickness. The strong effect of $V$ is particularly worth noting. The change in the front curvature as a result of the interaction of the particle and the deformable solid-liquid interface gives rise to the

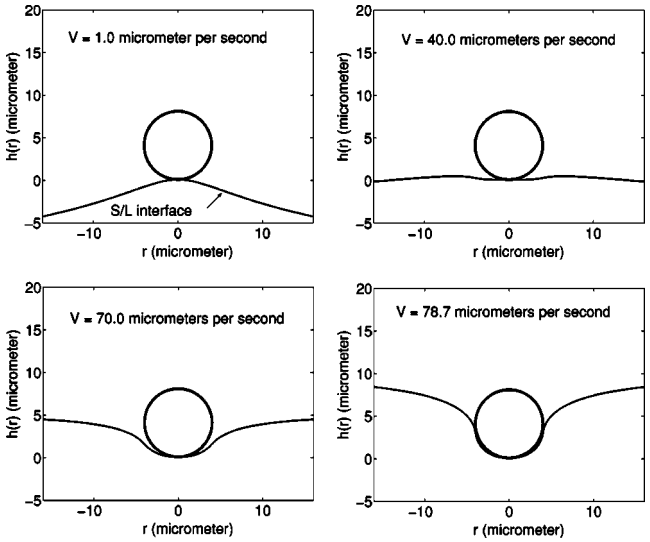


FIG. 8. Changes in the interface profile near the particle as function of the growth velocity $V$ for SCN immersed with air bubbles ($\alpha=0.0$); $a=4.0$ $\mu$m and $g_0=20$ Å.

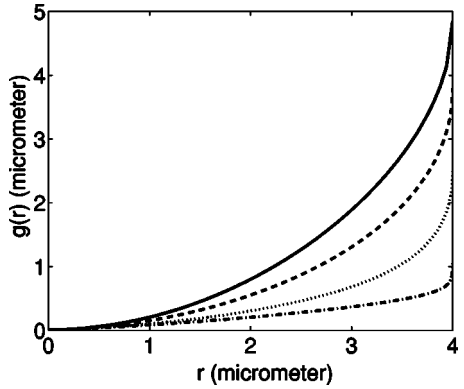


FIG. 9. Plot of the gap thickness $g(r)$ for a gas bubble with growth rates $V=1.0\ \mu\mathrm{m\,s^{-1}}$ (continuous line), $V=50.0\ \mu\mathrm{m\,s^{-1}}$ (dashed line), $V=70.0\ \mu\mathrm{m\,s^{-1}}$ (dotted line), and $V=78.7\ \mu\mathrm{m\,s^{-1}}$ (dash-dotted line).

pressure change $\mathcal{P}=\sigma_{sl}\mathcal{K}$ provided that changes in the pressure distribution in the solid are ignored. On using Eq. (13), we have

$$\mathcal{P}=-\frac{LGa^3}{T_m}\left(\frac{\alpha-1}{\alpha+2}\right)H(r)+\left(\frac{\mathcal{A}}{6\pi g^3(r)}-6\mu V\int_0^r\frac{x}{g^3(x)}dx\right)u(a-r). \tag{21}$$

This pressure change will, in turn, induce a force on the particle given by

$$\mathcal{F}=\frac{LGa^3}{T_m}\left(\frac{1-\alpha}{\alpha+2}\right)\int_0^\infty 2\pi rH(r)dr+\frac{\mathcal{A}}{3}\int_0^a\frac{r}{g^3(r)}dr-12\pi\mu V\int_0^a r\int_0^r\frac{x}{g^3(x)}dx. \tag{22}$$

The evaluation of the first term yields the expression for the thermal force, Eq. (1). This thermal force is evaluated by considering the pressure distribution in the gap to be the same as that at the interface, $z=0$. A more accurate evaluation requires using the pressure distribution at the particle-melt boundary, $z=S_-(r)\cup S_+(r)$, where $S_-(r)=h_\infty+a-\sqrt{a^2-r^2}$ and $S_+(r)=h_\infty+a+\sqrt{a^2-r^2}$. The distortion of the solid-liquid interface due to the thermal conductance contrast gives rise to a pressure change at the interface, $z=0$. This, in turn, induces a pressure distribution in the melt, $z>0$, and possibly a corresponding weak flow. Thus, the creeping flow equations are assumed applicable. The pressure distribution, $P(r,z)$, that satisfies Laplace's equation and takes the value $P(r,0)=LGa^3(1-\alpha)H(r)/T_m(\alpha+2)$ at the interface, is given by

$$P(r,z)=\frac{LGa^3(1-\alpha)[(h_\infty+a)-z]}{T_m(\alpha+2)\{[z-(h_\infty+a)]^2+r^2\}^{3/2}}.$$

Thus

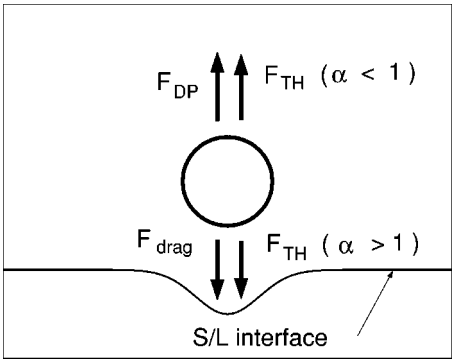


FIG. 10. Sketch of the forces acting on the particle. These are the disjoining pressure force $F_{DP}$, the drag force $F_{drag}$, and the thermal force $F_{TH}$. The latter pushes the particle against the front if $\alpha>1$ and pushes the particle away from the front if $\alpha<1$.

$$P(r,S_\pm(r))=\pm\frac{LG(1-\alpha)}{T_m(2+\alpha)}\sqrt{a^2-r^2}.$$

The thermal force acting on the particle is thus obtained by integrating the pressure over the surfaces $S_-$ and $S_+$. We obtain

$$F_{TH}=\frac{4\pi LGa^3}{3T_m}\left(\frac{1-\alpha}{2+\alpha}\right). \tag{23}$$

It differs from Eq. (1) by a factor of (2/3). The remaining two integral terms represent the disjoining pressure force, Eq. (2), and the viscous drag force, Eq. (3), respectively. These forces are sketched in Fig. 10. The evaluation of the drag and disjoining pressure forces depends on the calculated gap thickness profile $g(r)$. Estimates for the magnitude of these forces are often made by assuming a planar interface [10]. The gap thickness will then assume a parabolic profile and closed form formulas for the disjoining force and the hydrodynamic force can be obtained. They are

$$F_{DP}=\frac{a\mathcal{A}}{6g_0^2}\quad\text{and}\quad F_{drag}=\frac{6\pi\mu Va^2}{g_0}, \tag{24}$$

and were proposed by Verwey and Overbeek [27] and Brenner [28], respectively.

Consider a particle that is approached by the solid front at a velocity $V$. When the particle is less than a particle diameter from the front, it is subjected to the thermal force, Eq. (23). This force either pushes the particle against the front if $\alpha>1$ or pushes it away from the front if $\alpha<1$. The drag force, Eq. (3), acts in such a way as to oppose the motion of the particle. The competition between these two forces will determine whether or not the particle gets near enough to the front. In the affirmative, as the gap separation decreases, the disjoining pressure force becomes important, Eq. (2), and hence, the final outcome of this interaction will be determined from the competition of three forces. Otherwise, the particle remains ahead of the interface and the disjoining pressure never enters into play. An assessement of the magnitudes of the three forces is carried out and the results

TABLE I. Magnitudes of the disjoining pressure force $F_{DP}$, the drag force $F_{drag}$, the thermal force $F_{\mathrm{TH}}$, and the total force $\mathcal{F}$ in nanonewtons ($10^{-9}$ N) on a SiC particle of radius $a=4.0$ $\mu$m immersed in succinonitrile; $g_0=125$ Å and $G=10\,800$ K m$^{-1}$. The negative sign indicates an attractive force between the particle and the front.

| $V$ ($\mu$m s$^{-1}$) | $F_{DP}$ (nN) | $F_{drag}$ (nN) | $F_{TH}$ (nN) | $\mathcal{F}$ (nN) |
|---|---|---|---|---|
| 0.1 | 6.3 | −1.5 | −400.0 | −395.0 |
| 1.0 | 6.4 | −15.0 | −400.0 | −408.0 |
| 5.0 | 6.7 | −78.0 | −400.0 | −471.0 |
| 15.0 | 7.9 | −280.0 | −400.0 | −672.0 |
| 18.0 | 8.7 | −360.0 | −400.0 | −751.0 |
| 21.0 | 10.0 | −500.0 | −400.0 | −890.0 |

shown in Tables I–III. The case of an SiC particle of radius $a=4.0$ $\mu$m in SCN is presented in Table I for $g_0=125$ Å and $G=10\,800$ K m$^{-1}$. It is clear that the thermal force dominates the interaction over a wide range of growth rates in this particular case. The increase of $F_{DP}$ with $V$ is due to the decrease of the gap separation profile, $g(r)$, with $V$ as shown in Fig. 9. The decrease of $g(r)$ with $V$ also contributes to the increase of $F_{drag}$. The decrease of $g_0$ to 20 Å leads to an increase in the values for $F_{DP}$ but the resulting increase is not enough to balance those of $F_{drag}$ or $F_{TH}$ (Table II). Table III gives the results for the case of an air bubble in SCN. In this case, the thermal force is repulsive and dominates the interaction for low growth rates. When $V$ exceeds some value between 5 $\mu$m s$^{-1}$ and 10 $\mu$m s$^{-1}$, the magnitude of $F_{drag}$ exceeds that of $F_{TH}$ and the particle is pushed against the front. Note that Eqs. (24) yield $F_{DP}=17$ nN and $F_{drag}=0.4$ nN for the case given by Table III. Thus, Eqs. (24) underestimate the hydrodynamic force but approximate the disjoining force well. This is an indication that the disjoining force is effective only in the thin region near the origin; the interfacial deformations play a minor role.

## V. DISCUSSION AND CONCLUSIONS

We have formulated a steady state model to analyze the interaction of a colloidal particle with a solidifying interface in a microgravity environment. The particle is assumed to be spherical, smooth, and insoluble. The formulation of the model assumes a very slowly moving interface for two reasons. The first one has to do with the fact that at low solidification rates, the possibility of the onset of morphological instabilities is remote and the particle's presence constitutes the sole cause of interfacial distortions. The second reason has to do with the fact that, given that $Va/\kappa \ll 1$, the thermal field can be appoximated using the immobile interface condition. This is a standard approximation in such studies. The model includes the coupled effects due to the disjoining pressure, the hydrodynamic pressure, the deformability of the interface, and the modification of the thermal gradient due to the difference in thermal conductivities between the particle and the liquid.

TABLE II. Magnitudes of the disjoining pressure force $F_{DP}$, the drag force $F_{drag}$, the thermal force $F_{TH}$, and the total force $\mathcal{F}$ in nanonewtons on an SiC particle of radius $a=4.0$ $\mu$m immersed in succinonitrile: $g_0=20$ Å and $G=10\,800$ K m$^{-1}$.

| $V$ ($\mu$ m s$^{-1}$) | $F_{DP}$ (nN) | $F_{drag}$ (nN) | $F_{TH}$ (nN) | $\mathcal{F}$ (nN) |
|---|---|---|---|---|
| 0.1 | 15.0 | −3.4 | −400.0 | −388.0 |
| 1.0 | 15.0 | −36.0 | −400.0 | −421.0 |
| 5.0 | 17.0 | −200.0 | −400.0 | −583.0 |
| 7.0 | 18.0 | −300.0 | −400.0 | −682.0 |

TABLE III. Magnitudes of the disjoining pressure force $F_{DP}$, the drag force $F_{drag}$, the thermal force $F_{TH}$, and the total force $\mathcal{F}$ in nanonewtons for an air bubble of radius $a=4.0$ $\mu$m immersed in succinonitrile; $g_0=20$ Å and $G=10\,800$ K m$^{-1}$.

| $V$ ($\mu$ m s$^{-1}$) | $F_{DP}$ (nN) | $F_{drag}$ (nN) | $F_{TH}$ (nN) | $\mathcal{F}$ (nN) |
|---|---|---|---|---|
| 0.1 | 12.0 | −2.8 | 202.0 | 211.0 |
| 1.0 | 12.0 | −28.0 | 202.0 | 186.0 |
| 5.0 | 12.0 | −147.0 | 202.0 | 67.0 |
| 10.0 | 13.0 | −306.0 | 202.0 | −91.0 |
| 15.0 | 14.0 | −485.0 | 202.0 | −269.0 |
| 20.0 | 15.0 | −704.0 | 202.0 | −487.0 |

We have considered for study two systems for which experimental results are available for comparaison, namely, the solidification of SCN in the presence of either SiC particles or dissolved air bubbles. Our results show that for very low growth rates, $V<1.0$ $\mu$m s$^{-1}$, the shape of the crystal-melt interface depends primarily on the value of the thermal conductance ratio $\alpha$, i.e., the front shape is convex if $\alpha<1$ (air bubble) and concave if $\alpha>1$ (SiC particle). The case $\alpha=1$, planar interface, does not occur in practice. The disjoining pressure plays a role in the distortion of the interface whenever the gap separation is very thin and $V \ll 1$ $\mu$m s$^{-1}$. Its effect appears in the form of a peak (or a dimple) in the front's profile at the origin. This peak was investigated by Hadji [19,20] for the case $\alpha=1$. It was found that the front's curvature exhibits a logarithmic singularity at the origin. The cause of the singularity can be traced back to Eq. (13). With $V=0$ and $\alpha=1$, Eq. (13) exhibits a balance between the effects of the undercoolings due to the disjoining pressure and curvature. Note that while the disjoining pressure acts to increase the front's curvature, the Gibbs-Thomson effect acts to decrease it [20]. For the case at hand, $\alpha$ differs from unity and the interface profile consists of the superposition of two shapes: (i) a profile due to the thermal conductivity difference and of extent $O(a)$ and (ii) the tiny dimple, of the order of the gap thickness, due to the disjoining pressure effect provided the gap separation is small enough. The inclusion of a small amount of undercooling due to the hydrodynamic pressure is found to inhibit the dimple formation.

The increase in the growth rate is associated with dramatic changes in the morphology of the interface. In both setups, shown in Figs. 7 and 8, we observe the process of engulfment taking place as $V$ is increased. The sequences of profiles obtained as function of the growth rate bear a very

striking resemblance to those obtained experimentally for the same systems but under terrestrial conditions [24]. Thus, the simple model put forth in this paper seems to capture the main features of the particle-interface interaction. The same sequence of profiles leading to engulfment is also observed for the case of larger particles. However, we have discovered that the growth rate required to obtain a given profile decreases with $a$, i.e., smaller size particles require higher growth rates for engulfment in agreement with numerous experiments.

A systematic evaluation of the three fundamental forces involved in the particle-interface interaction in a microgravity environment has been carried out. These forces are the thermal force, $F_{TH}$, the disjoining pressure force, $F_{DP}$, and the hydrodynamic force, $F_{drag}$. The results of such an evaluation, shown in Tables I–III, seem to indicate that $F_{DP}$ is not large enough to affect the interaction in any realistic situation. This is a surprising result given that the disjoining pressure force has always been thought of as being one of the most important factor influencing the interaction. The tabulated results do show that the interaction is primarily determined by the competition between $F_{TH}$ and $F_{drag}$. For the SCN-SiC case depicted in Tables I and II, both $F_{TH}$ and $F_{drag}$ act to push the particle against the front while for the air bubble in SCN, it is deduced from Table III that a value for the growth rate exists below which the total force $\mathcal{F}$ is repulsive and above which it is attractive. This value of the growth rate is termed critical velocity. Uhlmann *et al.* [13] were the first authors to introduce this term to describe the predictions of their experiments. The latter consisted of analyzing the behavior of different types of particles, such as graphite, magnesium oxide, and silt of sizes varying from one to several micrometers and several types of matrix materials, typically ice water or organic materials. They observed that for any particle-matrix system, there exists a specific value for the solidification velocity, below which the particles are rejected in the melt and above which they are incorporated in the solid.

There has been a recent attempt at investigating the interaction between a particle and an advancing solid-liquid interface on the space shuttle Columbia [29]. Unfortunaltely, the experimental findings were of limited use, given that they did not yield a two-dimensional view of the solid-liquid interface. Hardware constraints led to a slanted interface which restricted the observation of the particles located at the lower edge near the interface [30]. The quantitative experimental validation of our predictions must await the performance of carefully controlled experiments in a microgravity environment.


[1] A. R. Kennedy and T. W. Clyne, Cast Metals **4**, 160 (1991).
[2] K. A. Jackson and B. Chalmers, J. Appl. Phys. **29**, 1178 (1958).
[3] C. Korber, G. Rau, M. D. Cosman, and E. G. Cravalho, J. Cryst. Growth **72**, 649 (1985).
[4] A. Endo, H. Chauhan, S. Egi, and Y. Shiohara, J. Mater. Sci. **11**, 795 (1996).
[5] G. Gay and M. A. Azouni, Crystal Growth & Design **2**, 135 (2002).
[6] A. A. Chernov and D. E. Temkin, in *Current Topics in Materials Science*, edited by E. Kaldis and H. J. Scheel (North-Holland, Amsterdam, 1977), Vol. 2, pp. 3–77.
[7] D. Li and A. W. Neumann, in *Applied Surface Thermodynamics,* edited by A. W. Neumann and J. K. Spelt (Dekker, New York, 1996), Vol. 63, pp. 557–629.
[8] A. M. Zubko, V. G. Lobanov, and V. V. Nikonova, Kristallographiya **18**, 385 (1973) [Sov. Phys. Crystallogr. **18**, 239 (1973)].
[9] A. A. Chernov, D. E. Temkin, and A. M. Mel'nikova, Kristallographiya **22**, 27 (1977) [Sov. Phys. Crystallogr. **22**, 656 (1977)].
[10] L. Hadji, Phys. Rev. E **64**, 051502 (2001).
[11] A. A. Chernov, D. E. Temkin, and A. M. Mel'nikova, Kristallographiya **21**, 652 (1976) [Sov. Phys. Crystallogr. **21**, 369 (1976)].
[12] S. Middleman, *Modeling Axisymmetric Flows: Dynamics of Films, Jets, and Drops* (Academic, San Diego, 1995).
[13] D. R. Uhlmann, B. Chalmers, and K. A. Jackson, J. Appl. Phys. **35**, 2986 (1964).
[14] J. Pötschke and V. Rodge, J. Cryst. Growth **94**, 726 (1989).
[15] R. Sasikumar, T. R. Ramamohan, and B. C. Pai, Acta Metall. **37**, 2085 (1989).
[16] P. Casses and M. A. Azouni, J. Cryst. Growth **130**, 13 (1993).
[17] R. Sasikumar and T. R. Ramamohan, Acta Metall. Mater. **39**, 517 (1991).
[18] S. Sen, W. F. Faukler, P. Curreri, and D. M. Stefanescu, Metall. Mater. Trans. A **28A**, 2129 (1997).
[19] L. Hadji, Europhys. Lett. **51**, 413 (2000).
[20] L. Hadji, Phys. Rev. E **65**, 022201 (2002).
[21] W. Kurz and D. J. Fisher, *Fundamentals of Solidification* (Trans Tech Publications, Zurich, 1989).
[22] J. S. Langer, Rev. Mod. Phys. **52**, 1 (1980).
[23] J. N. Israelachvili, *Intermolecular and Surface Forces* (Academic, London, 1991).
[24] D. M. Stefanescu, R. V. Phalnikar, H. Pang, S. Ahuja, and B. K. Dhindaw, ISIJ Int. **35**, 300 (1995).
[25] S. G. Yiantsios and R. H. Davis, J. Colloid Interface Sci. **144**, 412 (1991).
[26] V. Cristini, J. Blawzdziewicz, and M. Loewenberg, J. Fluid Mech. **366**, 259 (1998).
[27] E. J. Verwey and J. Th. G. Overbeek, *The Theory and Stability of Lyophobic Colloids* (Elsevier, New York, 1948), Vol. 18, pp. 239–241.
[28] H. Brenner, Chem. Eng. Sci. **16**, 242 (1961).
[29] D. M. Stefanescu, F. R. Juretzko, B. K. Dhindaw, A. Catalina, S. Sen, and P. A. Curreri, Metall. Mater. Trans. A **29A**, 1697 (1998).
[30] D. M. Stefanescu (private communication).